

Article

# Free Convection Heat Transfer and Entropy Generation in an Odd-Shaped Cavity Filled with a Cu-Al<sub>2</sub>O<sub>3</sub> Hybrid Nanofluid

Mohammad Ghalambaz <sup>1,2</sup>, Seyed Mohsen Hashem Zadeh <sup>3</sup>, Ali Veismoradi <sup>4</sup>, Mikhail A. Sheremet <sup>5,\*</sup> and Ioan Pop <sup>6</sup>

- <sup>1</sup> Metamaterials for Mechanical, Biomechanical and Multiphysical Applications Research Group, Ton Duc Thang University, Ho Chi Minh City 758307, Vietnam; mohammad.ghalambaz@tdtu.edu.vn
- <sup>2</sup> Faculty of Applied Sciences, Ton Duc Thang University, Ho Chi Minh City 758307, Vietnam
- <sup>3</sup> Department of Mechanical Engineering, Shahid Chamran University of Ahvaz, Ahvaz 61355, Iran; mohsen.hashemzadeh@gmail.com
- <sup>4</sup> Chemical Engineering Department, Ferdowsi University, Mashhad 91735, Iran; ali.veismoradi@mail.um.ac.ir
- <sup>5</sup> Laboratory on Convective Heat and Mass Transfer, Tomsk State University, 634050 Tomsk, Russia
- <sup>6</sup> Faculty of Mathematics and Computer Science, Babeş-Bolyai University, 400084 Cluj-Napoca, Romania; popm.ioan@yahoo.co.uk
- \* Correspondence: sheremet@math.tsu.ru; Tel.: +7-38-2252-9740

**Abstract:** The present paper aims to analyze the thermal convective heat transport and generated irreversibility of water-Cu-Al<sub>2</sub>O<sub>3</sub> hybrid nanosuspension in an odd-shaped cavity. The side walls are adiabatic, and the internal and external borders of the enclosure are isothermally kept at high and low temperatures of  $T_h$  and  $T_c$ , respectively. The control equations based on conservation laws are formulated in dimensionless form and worked out employing the Galerkin finite element technique. The outcomes are demonstrated using streamlines, isothermal lines, heatlines, isolines of Bejan number, as well as the rate of generated entropy and the Nusselt number. Impacts of the Rayleigh number, the hybrid nanoparticles concentration ( $\phi_{mf}$ ), the volume fraction of the Cu nanoparticles to  $\phi_{mf}$  ratio ( $\phi_r$ ), width ratio ( $WR$ ) have been surveyed and discussed. The results show that, for all magnitudes of Rayleigh numbers, increasing nanoparticles concentration intensifies the rate of entropy generation. Moreover, for high Rayleigh numbers, increasing  $WR$  enhances the rate of heat transport.

**Keywords:** free convection; Cu-hybrid nanofluid; odd-shaped cavity; entropy generation; heat lines; finite element method



**Citation:** Ghalambaz, M.; Hashem Zadeh, S.M.; Veismoradi, A.; Sheremet, M.A.; Pop, I. Free Convection Heat Transfer and Entropy Generation in an Odd-Shaped Cavity Filled with a Cu-Al<sub>2</sub>O<sub>3</sub> Hybrid Nanofluid. *Symmetry* **2021**, *13*, 122. <https://doi.org/10.3390/sym13010122>

Received: 13 December 2020

Accepted: 6 January 2021

Published: 12 January 2021

**Publisher's Note:** MDPI stays neutral with regard to jurisdictional claims in published maps and institutional affiliations.



**Copyright:** © 2021 by the authors. Licensee MDPI, Basel, Switzerland. This article is an open access article distributed under the terms and conditions of the Creative Commons Attribution (CC BY) license (<https://creativecommons.org/licenses/by/4.0/>).

## 1. Introduction

The interest in the field of heat transfer has increased considerably recently. While device performance and heat generation have gone up, the sizes of the components have shrunk. For instance, computer chips that are made today are at least several orders of magnitude smaller in size as compared to the past. Thus, the generated heat per surface area is growing continuously. Thus, novel designs with improved heat transfer capabilities are demanded to cool devices that produce large amounts of heat.

Heat transfer in enclosed geometries with various initial and boundary conditions have been a hot topic in the past few decades. This is because these types of geometries have been utilized extensively in real-life applications, such as the cooling of electronic devices, thermal design of buildings, lubrication and drying applications, furnace and nuclear reactors, biochemical, and food processing. Nonetheless, rectangular and square lid-driven cavities have been studied more because of their simplicity and applicability. As such, a large portion of convective heat transport in cavities' studies has been devoted to rectangular geometries.

Among all the commonly used approaches to enhance heat transfer efficiency, including the passive and active methods, the dispersion of nano-sized particles of highly

conductive material in the base working fluids seems to be both simpler and more promising. Hence, in recent years, many studies have focused on applying nanofluids in heat transfer devices, including solar collectors, electronics, nuclear reactors, food, glass, and others [1–5]. For instance, Abu-Nada and Chamkha [6] investigated the role of Cu nanoparticles, Rayleigh number, and aspect ratio of the cavity in free convection heat transfer of CuO-EG-Water nanofluid. They found that the aspect ratio of the enclosure considerably impacts the rate of heat transfer. Oztop and Abu-Nada [7] surveyed the free convection heat transfer problem of nanofluids in rectangular cavities. They [7] revealed that the average Nusselt number enhances as the volume fraction of the nanoparticles increases. Parvin and Chamkha [8] presented a thermal convective motion, energy transport, and entropy production in an odd-shaped chamber. The computational analysis on the influence of thermal convection and solid particle concentration on Nu, total entropy generation, and Be was performed in the chamber saturated with Cu-H<sub>2</sub>O nanosuspension, which concluded horizontal and vertical parts. Furthermore, the entropy production resulting from energy transference, streamlines, and isotherms is shown for different Ra and particle concentrations.

Hybrid nanofluids are a new type of nanofluids. Generally, these types of fluid can be prepared by two separate approaches: (a) dispersion of two (or even more) nanosized particles to a base fluid, and (b) by suspending the so-called hybrid (also composite) nanoparticles to a host liquid. The efficacy of hybrid nanosuspensions through their chemical-physical characteristics was tested and proved by many numerical and experimental studies. The properties and applicability of hybrid nanosuspensions were extensively reviewed in the literature [9–14]. Furthermore, the role of different hybrid nanoparticles on the natural, mixed, and forced convection heat transfer has been discussed in some published research studies on the boundary layer by Suresh et al. [15], Aly and Pop [16], Ismael et al. [17], Waini et al. [18,19], Roslan et al. [20], Khashi'ie et al. [21–23], Ali et al. [24], Khan et al. [25] and Liu et al. [26]. For example, according to the experimentations of Suresh et al. [15], by employing Cu–Al<sub>2</sub>O<sub>3</sub> hybrid nanofluid, the rate of heat transfer could be enhanced up to around 13.5%. Ismael et al. [17] numerically surveyed the irreversibility and heat transfer of Cu–Al<sub>2</sub>O<sub>3</sub> hybrid nanofluid in a lid-driven cavity. They reported that using hybrid nanofluids is promising for the improvement of heat transfer and reducing the size of heat transfer devices. Roslan et al. [20] investigated the mixed convection heat transfer of Al<sub>2</sub>O<sub>3</sub>-Cu-water hybrid nanofluids in a rectangular cavity. The top lid of the cavity was moving with a constant velocity, inducing a mixed convection flow. The results of Roslan et al. [20], in agreement with the outcomes of Roslan et al. [20], showed that the presence of hybrid nanoparticles improved the heat transfer. Following [20], Ali et al. [24] analyzed the mixed convection of the same hybrid nanofluid for a double lid-driven cavity, where both top and bottom lids were moving. This research also confirmed the heat transfer enhancement of using hybrid nanofluids.

With the above review, it can be clearly observed that the natural convection heat transfer of hybrid nanofluids is an important task that could be promising for reducing the size of heat transfer devices. The literature reviewed above shows that the heat transfer and energy generation of nanosuspensions have been addressed in many recent publications. However, the entropy generation and visualization of heat transfer paths (heat-lines) of hybrid nanofluids, and the shape of enclosures, are the influential aspects that have been overlooked in the literature and will be tackled in the present work.

## 2. Problem Physics

Free convective heat transport of Cu–H<sub>2</sub>O hybrid nanofluid in the region formed between a hot block and its chamber is schematically shown in Figure 1.

The vertical (or horizontal) length of the hot (or cold) surfaces is  $L$  (or  $L-W$ ). The width of the cavity is  $W$  and can vary to have different width ratios ( $W/L$ ). The temperature of the interior walls, shown in red in Figure 1, is isothermally kept constant at  $T_h$ , and the external walls, depicted in blue, are at the temperature of  $T_c$ . The remaining borders are assumed

to be adequately insulated. It is assumed that the circulation is steady, incompressible, laminar, and the radiation has no significant effect on the process.

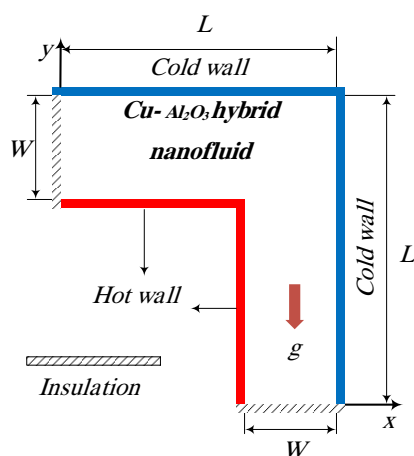


Figure 1. Schematic geometry of the problem.

2.1. Governing Equations

Under the above-mentioned assumptions, the control equations for the hybrid nanofluid, based on conservation laws, are [8,27]:

Continuity Equation:

$$\frac{\partial u}{\partial x} + \frac{\partial v}{\partial y} = 0 \tag{1}$$

Momentum Equation:

$$\rho_{hnf} \left( u \frac{\partial u}{\partial x} + v \frac{\partial u}{\partial y} \right) = -\frac{\partial p}{\partial x} + \mu_{hnf} \left( \frac{\partial^2 u}{\partial x^2} + \frac{\partial^2 u}{\partial y^2} \right) \tag{2}$$

$$\rho_{hnf} \left( u \frac{\partial v}{\partial x} + v \frac{\partial v}{\partial y} \right) = -\frac{\partial p}{\partial y} + \mu_{hnf} \left( \frac{\partial^2 v}{\partial x^2} + \frac{\partial^2 v}{\partial y^2} \right) + (\rho\beta)_{hnf} g(T - T_c) \tag{3}$$

Energy Equation:

$$(\rho c)_{hnf} \left( u \frac{\partial T}{\partial x} + v \frac{\partial T}{\partial y} \right) = k_{hnf} \left( \frac{\partial^2 T}{\partial x^2} + \frac{\partial^2 T}{\partial y^2} \right) \tag{4}$$

where  $u$  and  $v$  are the velocity components in  $x$  and  $y$  directions,  $T$  is the temperature of the hybrid nanofluid,  $g$  is the gravity and  $p$  is the pressure. The corresponding boundary conditions are

$$\begin{aligned} T &= T_h && \text{at the inner walls} \\ T &= T_c && \text{at the outer walls} \\ \frac{\partial T}{\partial n} &= 0 && \text{at the rest of the surfaces} \\ u &= v = 0 && \text{at all solid surfaces} \end{aligned} \tag{5}$$

2.2. Thermophysical Characteristics

In Equations (1)–(4),  $\rho_{hnf}$ ,  $(\rho c)_{hnf}$ ,  $\beta_{hnf}$  and  $\mu_{hnf}$  denote the density, thermal capacitance, heat expansion coefficient and dynamic viscosity of the nanofluid which could be calculated from the below relations [28]:

$$\mu_{hnf} = \mu_f (1 - \phi_{hnf})^{-2.5} \tag{6}$$

$$\rho_{hnf} = \rho_{Al_2O_3} \phi_{Al_2O_3} + \rho_{Cu} \phi_{Cu} + (1 - \phi_{hnf}) \rho_f \tag{7}$$

$$\frac{k_{hnf}}{k_f} = \frac{\left\{ \frac{\varphi_{Al_2O_3} k_{Al_2O_3} + \varphi_{Cu} k_{Cu}}{\varphi_{hnf}} + 2k_f + 2(\varphi_{Al_2O_3} k_{Al_2O_3} + \varphi_{Cu} k_{Cu}) - 2k_f \varphi_{hnf} \right\}}{\left\{ \frac{\varphi_{Al_2O_3} k_{Al_2O_3} + \varphi_{Cu} k_{Cu}}{\varphi_{hnf}} + 2k_f - (\varphi_{Al_2O_3} k_{Al_2O_3} + \varphi_{Cu} k_{Cu}) + k_f \varphi_{hnf} \right\}} \quad (8)$$

$$(\rho c)_{hnf} = \varphi_{Al_2O_3} (\rho c)_{Al_2O_3} + \varphi_{Cu} (\rho c)_{Cu} + (1 - \varphi_{hnf}) (\rho c)_f \quad (9)$$

$$(\rho \beta)_{hnf} = \varphi_{Al_2O_3} (\rho \beta)_{Al_2O_3} + \varphi_{Cu} (\rho \beta)_{Cu} + (1 - \varphi_{hnf}) (\rho \beta)_f \quad (10)$$

Here,  $\varphi_{hnf} = \varphi_{Al_2O_3} + \varphi_{Cu}$  is the volume fraction of the hybrid nanofluid. Moreover, the subscripts  $f$ ,  $Cu$ , and  $Al_2O_3$  refer to the base fluid,  $Cu$ , and  $Al_2O_3$  nanoparticles' properties, respectively. The physical characteristics of the hybrid nano-sized particles and water (as the host fluid) are gathered in Table 1.

**Table 1.** Thermal characteristics of  $Cu$  and  $Al_2O_3$  nanoparticles [29].

	$\rho$ (kg·m <sup>-3</sup> )	$c$ (J·kg <sup>-1</sup> ·K <sup>-1</sup> )	$k$ (W·m <sup>-1</sup> ·K <sup>-1</sup> )	$\alpha$ (m <sup>2</sup> ·s <sup>-1</sup> ) × 10 <sup>7</sup>	$\beta$ (K <sup>-1</sup> ) × 10 <sup>6</sup>
$Al_2O_3$	3970	765	40	131.7	25.5
$Cu$	8933	385	400	1163.1	50.1
Host fluid (water)	997.1	4179.0	0.613	1.47	210

### 2.3. Non-Dimensional Form of the Governing Equations

Equations (1)–(4) can be non-dimensionalized by introducing the below parameters:

$$X = \frac{x}{L}, Y = \frac{y}{L}, U = \frac{uL}{\nu_f}, V = \frac{vL}{\nu_f}, P = \frac{pL^2}{\rho_f \nu_f^2}, \theta = \frac{T - T_c}{T_h - T_c} \quad (11)$$

Substituting Equation (7) into Equations (1)–(4), results in the next equations

$$\frac{\partial U}{\partial X} + \frac{\partial V}{\partial Y} = 0 \quad (12)$$

$$\frac{\rho_{hnf}}{\rho_f} \left( U \frac{\partial U}{\partial X} + V \frac{\partial U}{\partial Y} \right) = -\frac{\partial P}{\partial X} + \frac{\mu_{hnf}}{\mu_f} \left( \frac{\partial^2 U}{\partial X^2} + \frac{\partial^2 U}{\partial Y^2} \right) \quad (13)$$

$$\frac{\rho_{hnf}}{\rho_f} \left( U \frac{\partial V}{\partial X} + V \frac{\partial V}{\partial Y} \right) = -\frac{\partial P}{\partial Y} + \frac{\mu_{hnf}}{\mu_f} \left( \frac{\partial^2 V}{\partial X^2} + \frac{\partial^2 V}{\partial Y^2} \right) + Ra \cdot Pr \frac{(\rho \beta)_{hnf}}{(\rho \beta)_f} \theta \quad (14)$$

$$\frac{(\rho c)_{hnf}}{(\rho c)_f} \left( U \frac{\partial \theta}{\partial X} + V \frac{\partial \theta}{\partial Y} \right) = \frac{k_{hnf}}{k_f} \left( \frac{\partial^2 \theta}{\partial X^2} + \frac{\partial^2 \theta}{\partial Y^2} \right) \quad (15)$$

where Rayleigh and Prandtl numbers are defined as

$$Ra = \frac{\rho \beta (T_h - T_c) L^3}{\alpha_f \nu_f} \quad (16)$$

$$Pr = \frac{C_p \mu_f}{k_f}$$

The boundary conditions (5) in non-dimensional form become

$$\begin{aligned} \theta &= 1 && \text{at the inner walls} \\ \theta &= 0 && \text{at the outer walls} \\ \frac{\partial \theta}{\partial N} &= 0 && \text{at the rest of the surfaces} \\ U &= V = 0 && \text{at all solid surfaces} \end{aligned} \quad (17)$$

#### 2.4. Rate of Heat Transfer

The parameter of interest in this research is the rate of energy transference from the hot border, which can be quantified by the average Nusselt number  $Nu_{avg}$  as:

$$Nu_{avg} = -\frac{1}{1-WR} \frac{k_{hmf}}{k_f} \left\{ \int_{Y=0}^{Y=1-WR} \frac{\partial \theta}{\partial X} \Big|_{X=1-WR} dY + \int_{X=0}^{X=1-WR} \frac{\partial \theta}{\partial Y} \Big|_{Y=1-WR} dX \right\} \quad (18)$$

### 3. Entropy Generation

The strength of generated entropy is expressed as:

$$s_{gen} = \frac{k_{hmf}}{T_0^2} \left[ \left( \frac{\partial T}{\partial x} \right)^2 + \left( \frac{\partial T}{\partial y} \right)^2 \right] + \frac{\mu_{hmf}}{T_0} \left[ 2 \left( \frac{\partial u}{\partial x} \right)^2 + 2 \left( \frac{\partial v}{\partial y} \right)^2 + \left( \frac{\partial u}{\partial y} + \frac{\partial v}{\partial x} \right)^2 \right] \quad (19)$$

The first term in the above equation is the energy transference component of entropy production. The second one indicates that the portion of generated entropy caused by friction of the hybrid nanofluid. The generated entropy could be transformed into the non-dimensional form using the below parameters [30,31]:

$$S = \frac{sT_0^2 L^2}{k_f(T_h - T_c)} \quad (20)$$

Equation (15) in the non-dimensional form reads as:

$$S_{gen} = S_{th} + S_{viscous} \quad (21)$$

where

$$S_{th} = \frac{k_{hmf}}{k_f} \left[ \left( \frac{\partial \theta}{\partial X} \right)^2 + \left( \frac{\partial \theta}{\partial Y} \right)^2 \right] \quad (22)$$

$$S_{viscous} = \chi \frac{\mu_{hmf}}{\mu_f} \left[ 2 \left( \frac{\partial U}{\partial X} \right)^2 + 2 \left( \frac{\partial V}{\partial Y} \right)^2 + \left( \frac{\partial U}{\partial X} + \frac{\partial V}{\partial Y} \right)^2 \right] \quad (23)$$

Here  $\chi$  is called the irreversibility function and can be defined as:

$$\chi = \frac{T_0 \mu_f}{k_f} \left[ \frac{L}{v_f(T_h - T_c)} \right]^2 \quad (24)$$

The ratio of generated entropy induced by energy transference to the total entropy production is called the Bejan number, which is

$$Be = \frac{S_{th}}{S_{gen}} \quad (25)$$

It is apparent that for  $Be > 0.5$  ( $Be < 0.5$ ), the irreversibility of the energy transference (fluid friction) governs the total entropy production.

### 4. Heat Function

The  $x$ - and  $y$ -derivatives of the heat function equal the energy flux components ( $j_x, j_y$ ) and for the hybrid nanofluid read as [32]:

$$j_x = \frac{\partial h}{\partial y} = (\rho c)_{hmf} u(T - T_c) - k_{hmf} \frac{\partial T}{\partial x} \quad (26)$$

$$j_y = -\frac{\partial h}{\partial x} = (\rho c)_{hmf} v(T - T_c) - k_{hmf} \frac{\partial T}{\partial y} \quad (27)$$

Using the non-dimensional heat function as  $H = \frac{h}{[\alpha_f(T_h - T_c)]}$ , the dimensionless form of the above equations is obtained as:

$$J_X = \frac{\partial H}{\partial Y} = \frac{(\rho c)_{hmf}}{(\rho c)_f} U\theta - \frac{k_{hmf}}{k_f} \frac{\partial \theta}{\partial X} \quad (28)$$

$$J_Y = -\frac{\partial H}{\partial X} = \frac{(\rho c)_{hmf}}{(\rho c)_f} V\theta - \frac{k_{hmf}}{k_f} \frac{\partial \theta}{\partial Y} \quad (29)$$

With a cross derivation, the dimensionless presentation of the heat function could be calculated as the following:

$$\frac{\partial^2 H}{\partial X^2} + \frac{\partial^2 H}{\partial Y^2} = \frac{(\rho c)_{hmf}}{(\rho c)_f} \left\{ \frac{\partial(V\theta)}{\partial X} - \frac{\partial(U\theta)}{\partial Y} \right\} \quad (30)$$

The boundary conditions for the above equation can be obtained by integrating over the Equations (23) or (24) and imposing the no-slip condition ( $U = V = 0$ ). In addition, the heat lines on the bottom wall can be arbitrary set to zero [32]:

on the bottom wall:

$$H(1 - WR \leq 0 \leq 1, 0) = 0 \quad (31)$$

on the inner walls:

$$H(1 - WR, 0 \leq Y \leq 1 - WR) = -\frac{k_{hmf}}{k_f} \int_0^Y \frac{\partial \theta}{\partial X} dY \text{ and} \\ H(0 \leq X \leq 1 - WR, 1 - WR) = \frac{k_{hmf}}{k_f} \int_0^X \frac{\partial \theta}{\partial Y} dX - \frac{k_{hmf}}{k_f} \int_0^{1-WR} \frac{\partial \theta}{\partial X} \Big|_{1-WR, 0 \leq Y \leq 1-WR} dY \quad (32)$$

on the outer walls:

$$H(1, 0 \leq Y \leq 1) = -\frac{k_{hmf}}{k_f} \int_0^Y \frac{\partial \theta}{\partial X} dY \text{ and} \\ H(0 \leq X \leq 1, 1) = \frac{k_{hmf}}{k_f} \int_0^X \frac{\partial \theta}{\partial Y} dX - \frac{k_{hmf}}{k_f} \int_0^1 \frac{\partial \theta}{\partial X} \Big|_{1, 0 \leq Y \leq 1} dY \quad (33)$$

on the right adiabatic wall:

$$H(0, 1 - WR \leq Y \leq 1) = Nu_{avg} \\ = -\frac{k_{hmf}}{k_f} \int_0^{1-WR} \frac{\partial \theta}{\partial Y} \Big|_{0 \leq X \leq 1-WR, 1-WR} dX \\ - \frac{k_{hmf}}{k_f} \int_0^{1-WR} \frac{\partial \theta}{\partial X} \Big|_{1-WR, 0 \leq Y \leq 1-WR} dY \quad (34)$$

The employed numerical method, details of the grid check and validations are discussed in the Appendices A and B.

## 5. Results and Discussion

In this section, different parameters including Rayleigh number ( $Ra = 10^3, 10^4$  and  $10^5$ ), width ratio ( $WR = W/L = 0.2, 0.3$  and  $0.4$ ), the concentration of the hybrid nanoparticles ( $0.0 \leq \phi_{hmf} \leq 0.05$ ) and the concentration of Cu to  $\phi_{hmf}$  ratio ( $0.0 \leq \phi_r = \phi_{Cu} / \phi_{hmf} \leq 1.0$ ) have been surveyed and discussed. Moreover, the Prandtl number  $Pr = 6.2$  is considered to be constant in all simulations.

Figure 2 shows the isotherms, heat lines, and streamlines in the cavity filled with hybrid nanosuspension for different  $Ra$  and  $WR$  values. Figure 2a represents the isotherms, which as seen, the isotherms are layered in the horizontal direction at  $Ra = 10^3$ . The layered arrangements of the isotherms confirm that conduction energy transference is the dominant mode of heat transport in the chamber. It should be noted that the isotherms signify the strength of the conduction heat transfer; for instance, it can be observed from Figure 2 that the conduction energy transference has larger values near the walls (especially the

hot walls). Conversely, the heat lines at  $Ra = 10^3$  and  $WR = 0.2$  show the perpendicular lines toward isotherms, and heat lines in this figure represent the routes of the energy transference from the hot border to the cold border with the conduction mechanism. Furthermore, the first row of Figure 2c demonstrates a vortex zone in the vertical part of the chamber, which represents a slight fluid velocity in this region. By increasing the  $WR$  from 0.2 to 0.3 at the same  $Ra$  (second row), the isotherms tend to separate as a result of conduction energy transference reduction. In this new state, the maximum value of the heat line is reduced from 9 to 5.5, and this reduction shows the lower energy transport strength in the cavity. Therefore, it can be concluded that the rate of energy transport from the hot border to the cold border decreases if the wall width increases when the conduction is the dominant phenomenon.

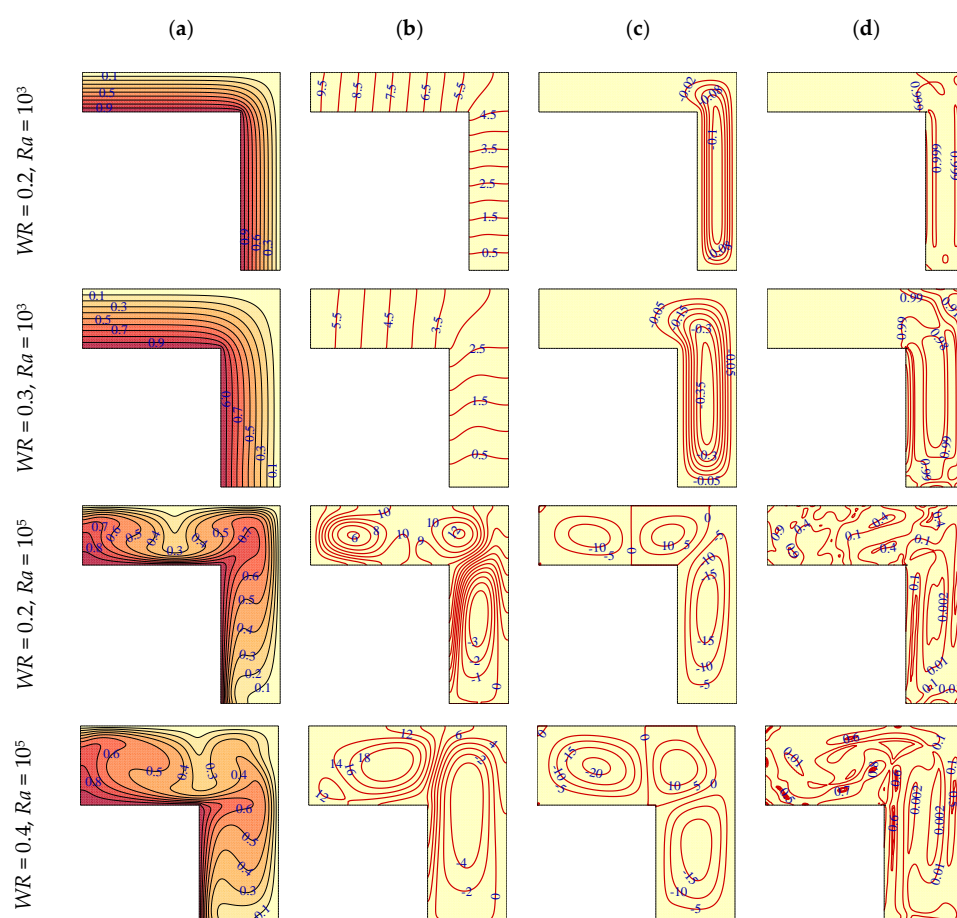


**Figure 2.** The impact of  $WR$  and  $Ra$  on (a) isotherms, (b) heat lines, (c) streamlines and (d) total isentropic lines when  $Pr = 6.2$ ,  $\phi_{mf} = 0.05$  and  $\phi_r = 0.5$ .

The uniformity of isotherms is gone when the  $Ra$  number is increased to  $10^5$  at the same  $WR = 0.3$  (third row), especially in the horizontal zone of the chamber. It depicts that the conduction energy transference is mainly restricted to the walls, and  $Ra$  increment leads to increasing buoyancy force. Moreover, the streamlines show different vortices at  $Ra = 10^5$  and  $WR = 0.3$ , and these vortices are started to evolve in a horizontal direction, and the routes of heat transfer are mainly similar to streamlines. Therefore, it can be concluded; the free convective energy transference now is the dominant mode in the cavity. In the last line of Figure 2, the effect of  $WR$  is depicted at the high value of  $Ra$ . By increasing the  $WR$  from 0.3 to 0.4 at the  $Ra = 10^5$ , the conduction effect on heat transfer is weakened, even in the cavity's vertical part. Furthermore, the stronger vortices and more extensive heat lines distribution, especially in the horizontal part, show the dominance convection heat transfer, which is boosted by increasing the wall width. It can be found from Figure 2

that the maximum value of the heat lines is raised in the high  $Ra$  when the wall width is increased. Therefore, increasing wall width has a direct influence on energy transference at the high  $Ra$ . Figure 2d shows the isentropic lines as the  $Be$  number is changed in the range between 0 and 1. It can be observed from the figures that the lines, with larger values, are close to walls. It shows in these areas the thermal entropy has mainly the same values as total entropy. In addition, some lines with lower values of  $Be$  are emerged in the middle of vertical cavity by increasing  $Ra$  and  $WR$  that show the effect of viscous entropy in these areas. Furthermore, these lines extend in horizontal part when the convective energy transport is the dominant mode in the chamber. Figure 3 shows the alteration of average  $Nu$  values against the total amount of nanoparticle volume fractions, with an equal proportion of Cu and  $Al_2O_3$  in the water-based fluid. It can be obtained from Figure 3a, that the  $Nu_{avg}$  has a more considerable value in the higher  $Ra$  as a result of natural convection increment, which was discussed in Figure 2. On the other hand, Figure 3a shows that the  $Nu_{avg}$  rises when a higher concentration of solid particles presents in the medium. The investigated nanoparticles in this research have a high heat transfer conduction coefficient, and the presence of these materials can enhance the conduction phenomena. For this reason, the same slopes are observed in Figure 3a, and this represents that the nanoparticles have the same and constant effect in different  $Ra$  values. Figure 3b shows that the  $Be$  number goes down when the  $Ra$  number is increased. For high  $Ra$ , the energy transport is enhanced. Therefore, the generated entropy due to energy transference increases, but it can be found from Figure 3b that the generated entropy caused by friction of the hybrid nanofluid has a higher value increment compared to  $S_{th}$  that leads to  $Be$  number reduction. However, nanoparticle volume fractions have no influence on the  $Be$  number in any values of the  $Ra$  (see Figure 3b). After increasing the nanoparticle volume fractions, heat transfer entropy and overall entropy both increased, so  $Be$  remained almost constant.

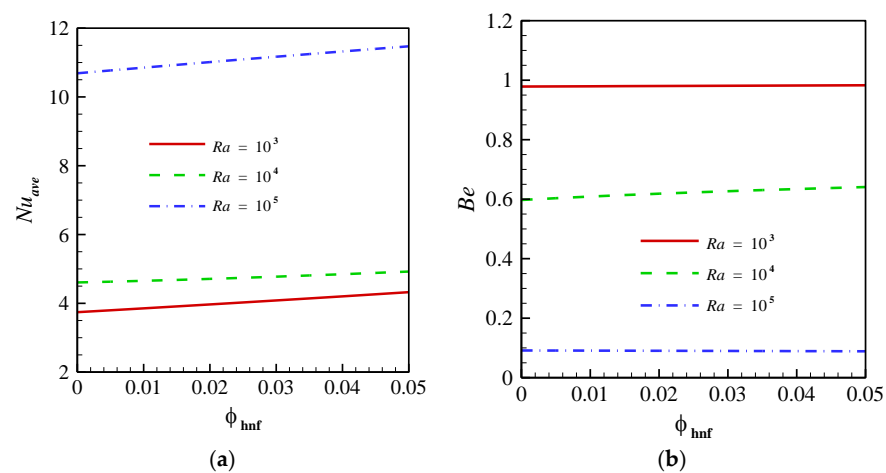


**Figure 3.** The variation of average (a)  $Nu$  and (b)  $Be$  numbers against nanofluid volume fractions in various  $Ra$  for  $Pr = 6.2$ ,  $WR = 0.3$  and  $\phi_r = 0.5$ .

Figures 4 and 5 demonstrate the influence of Cu nanoparticles concentration (in the constant value of  $\phi_r$ ) on the  $Nu_{avg}$  and  $Be$  numbers in different values of wall width. Figure 4a reveals that the percentage of Cu nanoparticle volume fractions has no considerable effect on the  $Nu_{avg}$ . Both Cu and  $Al_2O_3$  have a similar influence on hybrid nanofluid at  $Ra = 10^3$ . It can be seen from this Figure that the  $Nu_{avg}$  reduces considerably when the wall width is increased from 0.2 to 0.4. As previously described at  $Ra = 10^3$ , the conduction energy transference is the dominant regime; therefore, it is evident that the  $Nu_{avg}$  decreases according to the Fourier law when the  $WR$  increases. This reduction in heat transfer rate leads to entropy decrement, generated by heat transfer, and the  $Be$  reduction in Figure 4b is caused by this  $S_{th}$  alterations. Similar to the  $Nu_{avg}$ , the percentage of the Cu nanoparticle volume fractions has no considerable effect on  $Be$  number, because it does not affect the

rate of energy transference at the low  $Ra$ ; therefore, no entropy is generated by heat transfer and nanofluid frictions; then,  $Be$  remains constant at different values of  $\phi_r$ .

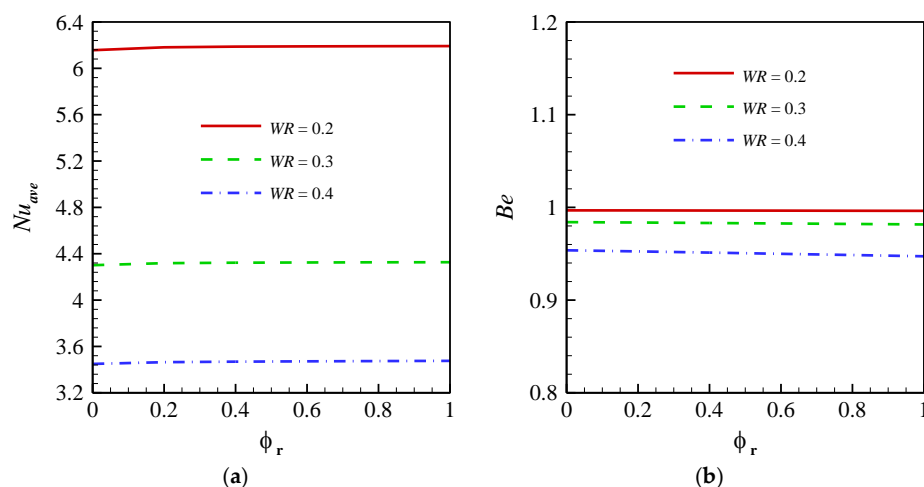


**Figure 4.** The variation of (a)  $Nu_{avg}$  and (b)  $Be$  numbers against  $\phi_r$  with different values of wall width ratio ( $\phi_{lmf} = 0.05$ ,  $Ra = 10^3$  and  $Pr = 6.2$ ).

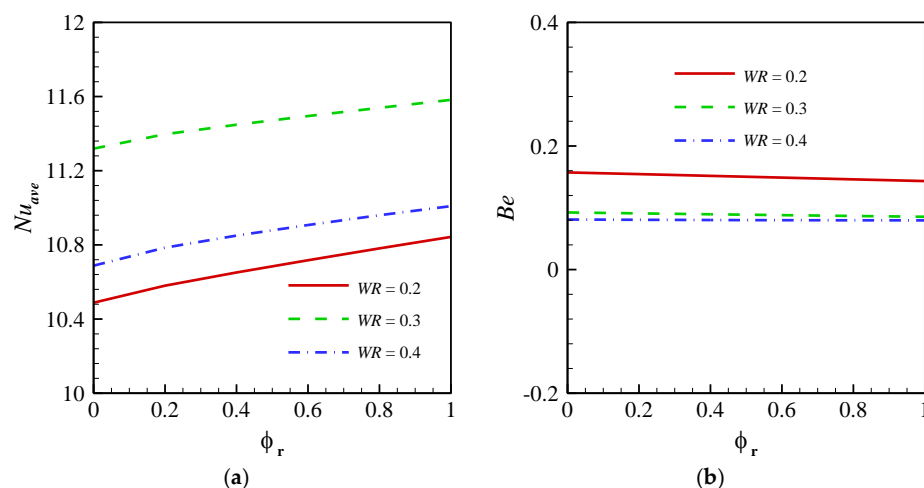


**Figure 5.** The variation of (a)  $Nu_{avg}$  and (b)  $Be$  numbers against  $\phi_r$  with different values of wall width ratio ( $\phi_{lmf} = 0.05$ ,  $Ra = 10^5$  and  $Pr = 6.2$ ).

Figure 5a shows that increasing the Cu particles in the hybrid nanofluid has a positive influence on energy transference at  $Ra = 10^5$ , in opposite results, as obtained from Figure 4a. This phenomenon can be attributed to the larger conduction heat transfer coefficient of Cu compared to  $Al_2O_3$  nanoparticles. By increasing the wall width from 0.2 to 0.3,  $Nu_{avg}$  is increased, as shown in Figure 5a. At  $WR = 0.3$ , the nanofluid can be circulated more easily in the cavity as a result of buoyancy force at  $Ra = 10^5$ . However, energy transference strength decreases considerably when  $WR$  increases to 0.4. Figure 5b shows similar results in Figure 4b, but for different reasons. The generated entropy caused by frictions increases when the wall width changes from 0.2 to 0.3 because of the nanofluid movement in the cavity. As for the previous results,  $Be$  number more depends on  $S_{viscous}$  than  $S_{th}$  at high  $Ra$  numbers. Therefore, a considerable reduction can be observed on  $Be$  number in Figure 5b when  $WR$  reaches 0.3. However, by increasing  $WR$  to 0.4, the convection effect is decreased (see Figure 5a); therefore, the nanofluid velocity decreases that leads to entropy reduction ( $S_{viscous}$ ). In this state, the  $S_{viscous}$  tends to  $S_{th}$  value, and because of this, the  $Be$  does not change noticeably at  $WR = 0.4$  compared to  $WR = 0.3$ . Figure 5b shows that the Cu nanoparticle volume fractions in hybrid nanofluid have no substantial effect on  $Be$  number

as a result of convection mechanisms dominance at high  $Ra$  numbers. However, Figure 5b shows that  $Be$  slightly decreases with  $\phi_r$  increment at  $WR = 0.2$ . These slight changes can be attributed to Cu density that has a larger value compared to  $Al_2O_3$ . The greater density at high  $Ra$  with a narrow wall width leads to increase entropy caused by friction factors and decrease  $Be$  number.

Figure 6 shows the influence of the  $Ra$  and the hybrid nanoparticles' concentration on the averaged of produced entropy. As previously mentioned, by increasing the  $Ra$  number, the buoyancy force intensifies, and hence, the average velocity and the rate of heat transfer in the enclosure increase (See Equations (22) and (23)). As a result, the velocity and temperature gradient are enhanced, and the generated entropy increases. As can be seen from Figure 6a,b, increasing the Rayleigh number has a considerable impact on both components of the produced entropy. It is evident that for low Rayleigh numbers, the friction share of entropy is almost feeble and the entropy generation is mainly controlled by the heat transfer mechanism. However, in high Rayleigh numbers,  $S_{viscous}$  overtakes its counterpart,  $S_{th}$  and the entropy generation induced by the friction of the hybrid nanofluid completely prevails. On the other hand, increasing the volume fraction of the hybrid nanoparticles, according to Equations (6) and (8) leads to the increment of the thermal conductivity and also the viscosity of the suspension. Hence, it slightly enhances the  $S_{th}$  (See Equation (22)) and  $S_{viscous}$  (See Equation (23)). Finally, Figure 6c represents the final result that the volume fraction of the hybrid nanoparticles, as well as the  $Ra$  number, have a direct influence on the total generated entropy in the cavity; however, the impact of the Rayleigh number (buoyancy force) is more substantial than the  $\phi_{hnf}$ .

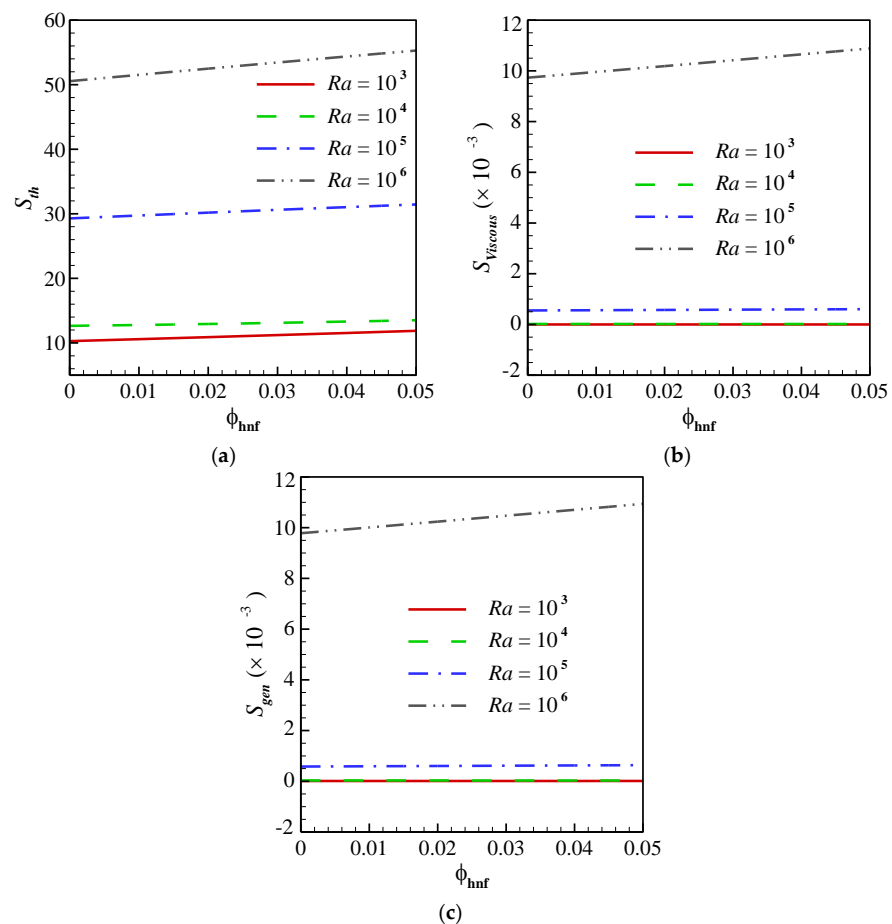


**Figure 6.** The impact of  $Ra$  and hybrid nanoparticles concentration on (a) entropy production due to energy transference, (b) the portion of generated entropy caused by friction of the hybrid nanofluid, and (c) total entropy production for  $WR = 0.3$ ,  $Pr = 6.2$  and  $\phi_r = 0.5$ .

## 6. Conclusions

The thermo-gravitational convection of water-Cu-Al<sub>2</sub>O<sub>3</sub> in an enclosed cavity was investigated. The enclosed cavity concluded two vertical and horizontal parts, and the heat was transferred from the left vertical border and bottom horizontal border toward other directions. The Cu and Al<sub>2</sub>O<sub>3</sub> nanoparticles were chosen as composite nanoparticles. Then, the different volume fractions of hybrid nanoparticles and their proportion were investigated on the energy transference. Furthermore, the effect of *Ra* and wall width and their relationship with nanoparticle volume fractions were studied as two other important factors, which affect the energy transference and generated entropy in the chamber. The conclusions are:

- Hybrid nanoparticles enhanced energy transport when the conduction mechanism was dominant. Conversely, they had no significant influence on convective transport;
- The wall-width ratio (*WR*) is a parameter that can have a different influence on the energy transference rate in different conditions. Increasing the wall width led to a reduction of the energy transference rate at low *Ra* (10<sup>3</sup>) owing to the dominant conduction heat transfer mechanism;
- *WR* had a positive influence on energy transference at high *Ra* (10<sup>5</sup>) when *WR* was increased from 0.2 to 0.3. However, a further increase of wall width reduced the heat transfer in the cavity when *WR* > 0.4, and therefore, an optimum wall width can enhance the heat transfer at high *Ra*;
- At *Ra* = 10<sup>3</sup>, the nanoparticles of Cu and Al<sub>2</sub>O<sub>3</sub> had a similar effect on nanofluid in the range of  $\phi_{hnf} = 0-0.05$ , and they enhanced the strength of energy transference to be the same as each other. Conversely, Cu nanoparticles had a stronger impact on heat transfer compared to Al<sub>2</sub>O<sub>3</sub> in convection heat transfer at *Ra* = 10<sup>5</sup>;
- *Ra* and  $\phi_{hnf}$  both could enhance generated thermal and viscous entropy, however, *Ra* had a more intensive influence on generated entropy in the cavity.

**Author Contributions:** Conceptualization, M.G., S.M.H.Z., A.V., I.P., M.A.S.; methodology, M.G., S.M.H.Z., A.V., I.P., M.A.S.; software, M.G.; validation, M.G.; investigation, M.G., S.M.H.Z., A.V., I.P., M.A.S.; writing—original draft preparation, M.G., S.M.H.Z., A.V., I.P., M.A.S.; writing—review and editing, M.G., S.M.H.Z., A.V., I.P., M.A.S. All authors have read and agreed to the published version of the manuscript.

**Funding:** This research received no external funding.

**Institutional Review Board Statement:** Not applicable.

**Informed Consent Statement:** Not applicable.

**Data Availability Statement:** Data will be available on request.

**Conflicts of Interest:** The authors declare no conflict of interest.

## Appendix A. Numerical Approach and Grid Check

The set of non-linear, coupled, and non-dimensional equations discussed above, has been worked out with the Galerkin finite element technique. The method has been well explained in [33]. To replace the pressure terms in the equation of momentum, the penalty parameter is defined as [33,34]:

$$P = -\chi \left( \frac{\partial U}{\partial X} + \frac{\partial V}{\partial Y} \right) \quad (\text{A1})$$

The mass conservation equation will be satisfied automatically when  $\chi$  is adequately high. By replacing the pressure terms with the above-defined penalty parameter, the momentum equations read:

$$\frac{\rho_{hnf}}{\rho_f} \left( U \frac{\partial U}{\partial X} + V \frac{\partial U}{\partial Y} \right) = \chi \frac{\partial}{\partial X} \left( \frac{\partial U}{\partial X} + \frac{\partial V}{\partial Y} \right) + \frac{\mu_{hnf}}{\mu_f} \left( \frac{\partial^2 U}{\partial X^2} + \frac{\partial^2 U}{\partial Y^2} \right) \quad (\text{A2})$$

$$\frac{\rho_{hmf}}{\rho_f} \left( U \frac{\partial V}{\partial X} + V \frac{\partial U}{\partial Y} \right) = \chi \frac{\partial}{\partial Y} \left( \frac{\partial U}{\partial X} + \frac{\partial V}{\partial Y} \right) + \frac{\mu_{hmf}}{\mu_f} \left( \frac{\partial^2 V}{\partial X^2} + \frac{\partial^2 U}{\partial Y^2} \right) + Ra \cdot Pr \frac{(\rho\beta)_{hmf}}{(\rho\beta)_f} \theta \quad (A3)$$

A basis function  $\left( \zeta_k |_{k=1}^N \right)$  is used to expand all the existing variables  $(U, V, \theta)$  within the computational domain:

$$U \approx \sum_{k=1}^N U_k \zeta_k(X, Y), V \approx \sum_{k=1}^N V_k \zeta_k(X, Y), \theta \approx \sum_{k=1}^N \theta_k \zeta_k(X, Y) \quad (A4)$$

By applying the Galerkin finite element technique, the following set of residual equations will be received for the inner nodes:

$$\begin{aligned} R_i^1 = & \frac{\rho_{hmf}}{\rho_f} \sum_{k=1}^N U_k \int_{\Omega} \left[ \left( \sum_{k=1}^N U_k \zeta_k \right) \frac{\partial \zeta_k}{\partial X} + \left( \sum_{k=1}^N V_k \zeta_k \right) \frac{\partial \zeta_k}{\partial Y} \right] \zeta_i dXdY + \\ & \chi \sum_{k=1}^N U_k \int_{\Omega} \frac{\partial \zeta_i}{\partial X} \frac{\partial \zeta_k}{\partial X} dXdY + \chi \sum_{k=1}^N V_k \int_{\Omega} \frac{\partial \zeta_i}{\partial X} \frac{\partial \zeta_k}{\partial Y} dXdY + \\ & \frac{\mu_{hmf}}{\mu_f} \sum_{k=1}^N U_k \int_{\Omega} \left[ \frac{\partial \zeta_i}{\partial X} \frac{\partial \zeta_k}{\partial X} + \frac{\partial \zeta_i}{\partial Y} \frac{\partial \zeta_k}{\partial Y} \right] dXdY \end{aligned} \quad (A5)$$

$$\begin{aligned} R_i^2 = & \frac{\rho_{hmf}}{\rho_f} \sum_{k=1}^N V_k \int_{\Omega} \left[ \left( \sum_{k=1}^N U_k \zeta_k \right) \frac{\partial \zeta_k}{\partial X} + \left( \sum_{k=1}^N V_k \zeta_k \right) \frac{\partial \zeta_k}{\partial Y} \right] \zeta_i dXdY + \\ & \chi \sum_{k=1}^N U_k \int_{\Omega} \frac{\partial \zeta_i}{\partial Y} \frac{\partial \zeta_k}{\partial X} dXdY + \chi \sum_{k=1}^N V_k \int_{\Omega} \frac{\partial \zeta_i}{\partial Y} \frac{\partial \zeta_k}{\partial Y} dXdY + \\ & \frac{\mu_{hmf}}{\mu_f} \sum_{k=1}^N V_k \int_{\Omega} \left[ \frac{\partial \zeta_i}{\partial X} \frac{\partial \zeta_k}{\partial X} + \frac{\partial \zeta_i}{\partial Y} \frac{\partial \zeta_k}{\partial Y} \right] dXdY + RaPr \frac{(\rho\beta)_{hmf}}{(\rho\beta)_f} \int_{\Omega} \sum_{k=1}^N \theta_k \zeta_k(X, Y) \end{aligned} \quad (A6)$$

$$\begin{aligned} R_i^3 = & \frac{(\rho c)_{hmf}}{(\rho c)_f} \sum_{k=1}^N \theta_k \int_{\Omega} \left[ \left( \sum_{k=1}^N U_k \zeta_k \right) \frac{\partial \zeta_k}{\partial X} + \left( \sum_{k=1}^N V_k \zeta_k \right) \frac{\partial \zeta_k}{\partial Y} \right] \zeta_i dXdY \\ & + \frac{k_{hmf}}{k_f} \sum_{k=1}^N \theta_k \int_{\Omega} \left[ \frac{\partial \zeta_i}{\partial X} \frac{\partial \zeta_k}{\partial X} + \frac{\partial \zeta_i}{\partial Y} \frac{\partial \zeta_k}{\partial Y} \right] dXdY \end{aligned} \quad (A7)$$

It should be noted that as the solutions of heat function and stream function equations could be obtained from post-processing, there is no need to solve these (and evaluate their residual equations) along with the other equations. Moreover, the process stops iterating when  $\sqrt{(R_i^1)^2 + (R_i^2)^2 + (R_i^3)^2} \leq 10^{-6}$  is reached.

As presented in Table A1, the average  $Nu$  and the total generated entropy obtained by five different grid densities are compared to ensure that the outcomes are grid-independent. Structured grids with equal length and height ( $\Delta x = \Delta y$ ) are used for grid check. The error percentage for  $Nu_{avg}$  and the total generated entropy has been obtained as:

$$Err_{\frac{Nu}{S_{gen}}} = 100 \times \left| \frac{\left( \frac{Nu}{S_{gen}} \right)_n - \left( \frac{Nu}{S_{gen}} \right)_{n-1}}{\left( \frac{Nu}{S_{gen}} \right)_{n-1}} \right| \quad (A8)$$

It can be seen that the results of the employed case No. 3 with 7344 ( $\Delta x = \Delta y = 1.0/120$ ) have admissible accuracy and hence, has been employed in all of the simulations. In addition, a view of the employed gird (case 3) is depicted in Figure A1.

**Table A1.** Grid check for  $Nu_{avg}$  and  $S_{gen}$  ( $Ra = 10^5, Pr = 6.2, \phi_{hmf} = 0.05, WR = 0.3, \phi_r = 0.5$ ).

Case Study (n)	No. of Elements	$Nu_{avg}$	$Err_{Nu}$ (%)	$S_{gen}$	$Err_{S_{gen}}$ (%)
1	3264	11.025	–	593.70	–
2	5100	11.022	0.027	596.68	0.499
3	7344	11.020	0.018	598.33	0.276
4	9996	11.019	0.009	599.33	0.167
5	13,056	11.019	0.001	599.98	0.108

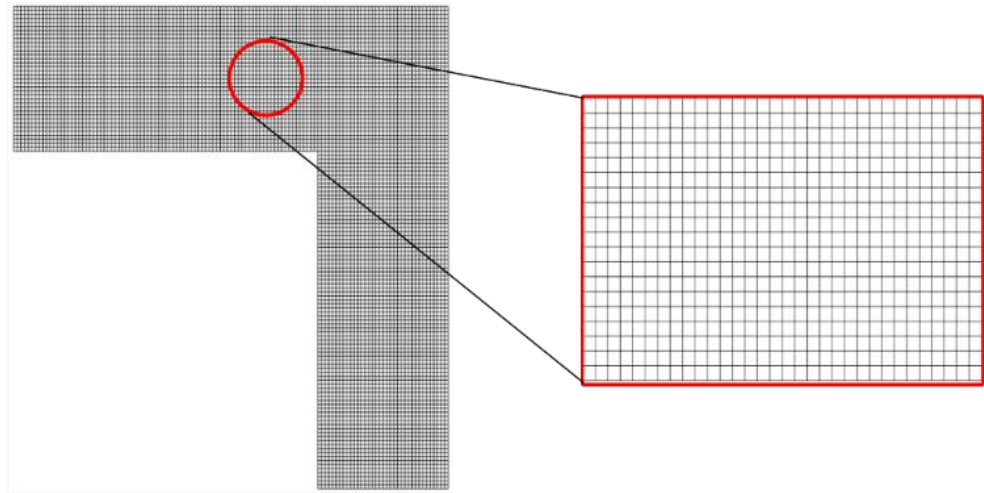


Figure A1. The utilized grid with 7344 elements.

### Appendix B. Validation of the Numerical Code

The validity of the developed finite element code should be checked to ensure the accuracy and correctness of the results. As such, three different research studies have been chosen and their outcomes have been re-stimulated to guarantee that all aspects of the code are fine and error-free. In Figure A2, a comparison is performed between the streamlines and isotherms of this research with another one shown by Nithiarasu et al. [35]. In [35], the buoyancy-driven flow of a simple flow has been addressed. The boundary conditions and geometry of this research are the same as the present one. It is evident that the patterns of streamlines and the isotherms are in quite a resemblance with [35], indicating that the developed code can accurately analyze the circulation and energy transference in the cavity.

In addition, to check that the equations governing the thermophysical characteristics of the nanofluid are appropriately implemented, the code has been further validated against a survey published by Kahveci [36] on the thermo-gravitational convection of nanosuspension in a chamber. In this research, the nano-sized particles are supposed to be easily fluidized, and hence, the solid-liquid two-phase flow of the nanoliquid is assumed to be homogenous and behaves as a single-phase fluid. The side walls in [36] are set to a temperature drop, and the upper and lower borders are adiabatic. The base fluid in work done by Kahveci [36] is water ( $Pr = 6.2$ ), and the impact of dispersion of different nanoparticles (including Cu, Ag, CuO, Al<sub>2</sub>O<sub>3</sub> and TiO<sub>2</sub>) on the circulation pattern and the rate of energy transference has been evaluated. Figure A3 depicts the comparison between the outcomes of Kahveci [36] and the present research for the dependency of the  $Nu_{avg}$  on the concentration of Al<sub>2</sub>O<sub>3</sub> nano-sized particles. It is apparent that the obtained values of the  $Nu_{avg}$  coincide with the data of Kahveci [36], representing a finite element code that can appropriately simulate the thermal convective energy transference of nanoliquids in a confined chamber.

As the final step, two more verifications have been performed to ensure that both entropy generation terms and the heat lines are correctly calculated. Figure A4 shows the isentropic lines and isolines of local Bejan number for the work done by Ilis [37] and the current study. In [37], the entropy generation resulting from free convective transport in a square chamber has been analyzed. The imposed boundary conditions are exactly the same as [36]. It is evident that both  $S_{gen}$  and  $Be$  are correctly calculated, and the values of similar isolines are quite similar. Finally, the survey of Deng and Tang [38], shown in Figure A5, has been utilized to check the validity of the solved heat function equation. The employed boundary conditions in [38] are exactly the same as [36,37], except that a solid rectangular solid is placed in the center of the cavity, and an extra energy equation for the solid block needs to be solved. As seen, the heat lines are in acceptable agreement with those presented by Deng and Tang [38].

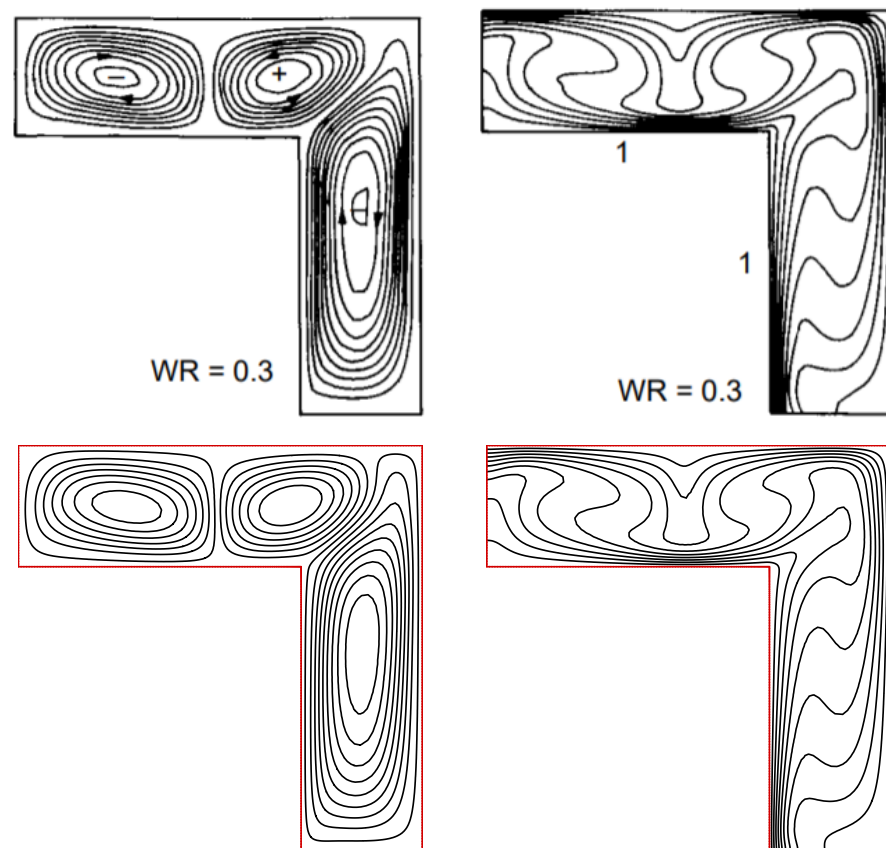


Figure A2. Comparison between the isolines of air ( $Ra = 10^6$ ,  $Pr = 0.71$ ,  $WR = 0.3$ ) for the present work and another one presented by Nithiarasu et al. [35].

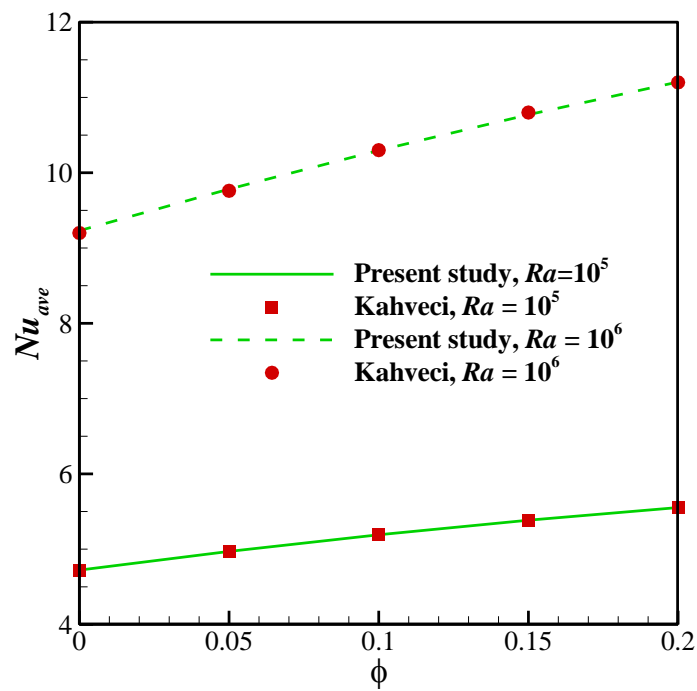
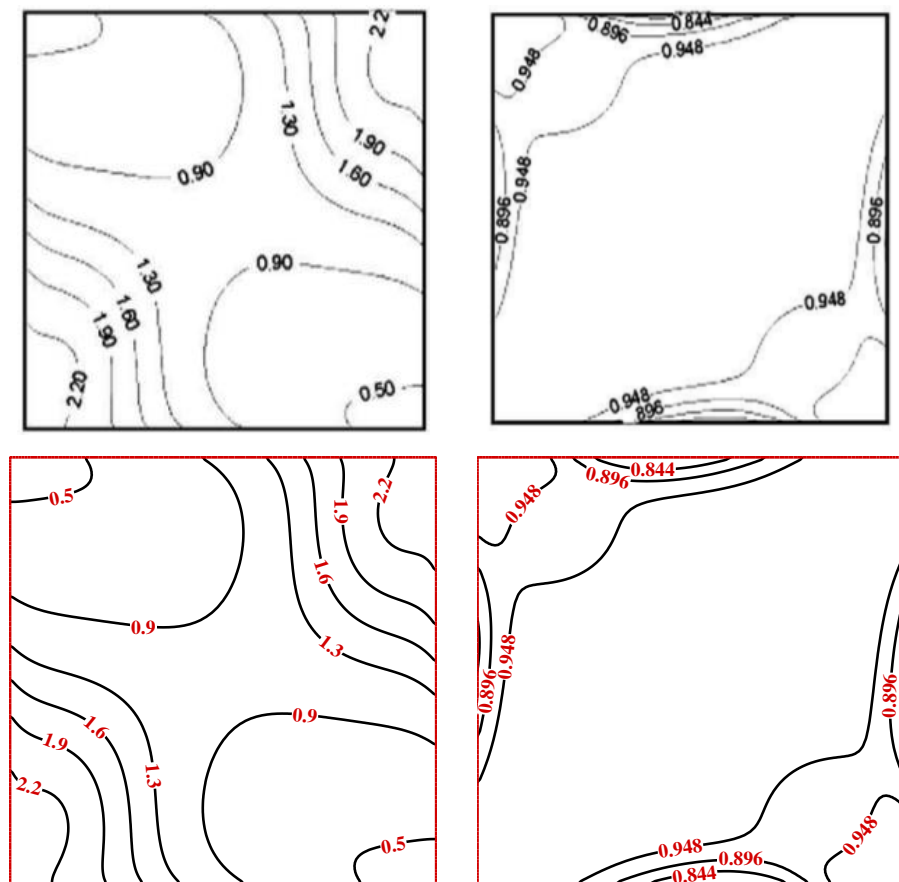
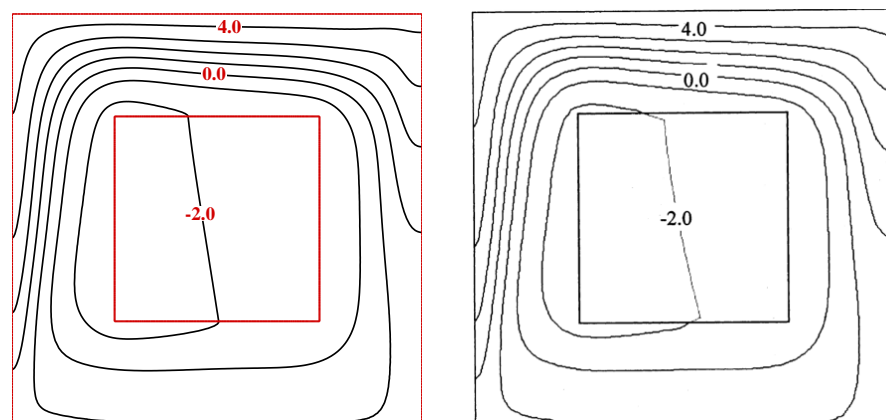


Figure A3. Influence of  $Al_2O_3$  nanoparticles volume fraction on the  $Nu_{avg}$  ( $Pr = 6.2$ ,  $\beta = 0.02$ ,  $\theta = 0^\circ$ ): Comparison between the present work and outcomes of Kahveci [36].



**Figure A4.** Comparison between (left) the total entropy production and (right) the local Bejan number ( $Ra = 10^6$ ,  $Pr = 0.71$ ,  $WR = 0.3$ ): Ilis [37] and the present research.



**Figure A5.** Comparison between the patterns of heat lines obtained by Deng and Tang [38] and the present work ( $Ra = 10^5$ ,  $Pr = 0.71$ ).

## References

1. Mansour, M.A.; Mohamed, R.A.; Abd-Elaziz, M.M.; Ahmed, S.E. Numerical simulation of mixed convection flows in a square lid-driven cavity partially heated from below using nanofluid. *Int. Commun. Heat Mass Transf.* **2010**, *37*, 1504–1512. [\[CrossRef\]](#)
2. Bhattacharya, M.; Basak, T.; Oztop, H.F.; Varol, Y. Mixed convection and role of multiple solutions in lid-driven trapezoidal enclosures. *Int. J. Heat Mass Transf.* **2013**, *63*, 366–388. [\[CrossRef\]](#)
3. Das, S.K.; Choi, S.U.; Yu, W.; Pradeep, T. *Nanofluids: Science and Technology*; John Wiley & Sons: Hoboken, NJ, USA, 2007.
4. Tyagi, H. *Radiative and Combustion Properties of Nanoparticle-Laden Liquids*; Arizona State University: Phoenix, AZ, USA, 2008.

5. Mahian, O.; Kianifar, A.; Kalogirou, S.A.; Pop, I.; Wongwises, S. A review of the applications of nanofluids in solar energy. *Int. J. Heat Mass Transf.* **2013**, *57*, 582–594. [[CrossRef](#)]
6. Abu-Nada, E.; Masoud, Z.; Oztop, H.F.; Campo, A. Effect of nanofluid variable properties on natural convection in enclosures. *Int. J. Therm. Sci.* **2010**, *49*, 479–491. [[CrossRef](#)]
7. Oztop, H.F.; Abu-Nada, E. Numerical study of natural convection in partially heated rectangular enclosures filled with nanofluids. *Int. J. Heat Fluid Flow* **2008**, *29*, 1326–1336. [[CrossRef](#)]
8. Parvin, S.; Chamkha, A.J. An analysis on free convection flow, heat transfer and entropy generation in an odd-shaped cavity filled with nanofluid. *Int. Commun. Heat Mass Transf.* **2014**, *54*, 8–17. [[CrossRef](#)]
9. Sarkar, J.; Ghosh, P.; Adil, A. A review on hybrid nanofluids: Recent research, development and applications. *Renew. Sustain. Energy Rev.* **2015**, *43*, 164–177. [[CrossRef](#)]
10. Sidik, N.A.C.; Adamu, I.M.; Jamil, M.M.; Kefayati, G.H.R.; Mamat, R.; Najafi, G. Recent progress on hybrid nanofluids in heat transfer applications: A comprehensive review. *Int. Commun. Heat Mass Transf.* **2016**, *78*, 68–79. [[CrossRef](#)]
11. Sundar, L.S.; Sharma, K.V.; Singh, M.K.; Sousa, A.C.M. Hybrid nanofluids preparation, thermal properties, heat transfer and friction factor—A review. *Renew. Sustain. Energy Rev.* **2017**, *68*, 185–198. [[CrossRef](#)]
12. Ranga Babu, J.A.; Kumar, K.K.; Srinivasa Rao, S. State-of-art review on hybrid nanofluids. *Renew. Sustain. Energy Rev.* **2017**, *77*, 551–565. [[CrossRef](#)]
13. Huminic, G.; Huminic, A. Hybrid nanofluids for heat transfer applications—A state-of-the-art review. *Int. J. Heat Mass Transf.* **2018**, *125*, 82–103. [[CrossRef](#)]
14. Sajid, M.U.; Ali, H.M. Thermal conductivity of hybrid nanofluids: A critical review. *Int. J. Heat Mass Transf.* **2018**, *126*, 211–234. [[CrossRef](#)]
15. Suresh, S.; Venkitaraj, K.P.; Selvakumar, P.; Chandrasekar, M. Effect of Al<sub>2</sub>O<sub>3</sub>–Cu/water hybrid nanofluid in heat transfer. *Exp. Therm. Fluid Sci.* **2012**, *38*, 54–60. [[CrossRef](#)]
16. Aly, E.H.; Pop, I. MHD flow and heat transfer over a permeable stretching/shrinking sheet in a hybrid nanofluid with a convective boundary condition. *Int. J. Numer. Methods Heat Fluid Flow* **2019**, *29*. [[CrossRef](#)]
17. Ismael, M.A.; Armaghani, T.; Chamkha, A.J. Mixed Convection and Entropy Generation in a Lid-Driven Cavity Filled with a Hybrid Nanofluid and Heated by a Triangular Solid. *Heat Trans. Res.* **2018**, *49*, 1645–1665. [[CrossRef](#)]
18. Waini, I.; Ishak, A.; Groşan, T.; Pop, I. Mixed convection of a hybrid nanofluid flow along a vertical surface embedded in a porous medium. *Int. Commun. Heat Mass Transf.* **2020**, *114*, 104565. [[CrossRef](#)]
19. Waini, I.; Ishak, A.; Pop, I. Transpiration effects on hybrid nanofluid flow and heat transfer over a stretching/shrinking sheet with uniform shear flow. *Alex. Eng. J.* **2020**, *59*, 91–99. [[CrossRef](#)]
20. Roslan, R.; Ali, I.; Alsabery, A.I.; Bakar, N. Mixed Convection in a Lid-Driven Horizontal Rectangular Cavity Filled with Hybrid Nanofluid By Finite Volume Method. *J. Adv. Res. Micro Nano Eng.* **2020**, *1*, 38–49.
21. Khashi'ie, N.S.; Md Arifin, N.; Pop, I. Mixed Convective Stagnation Point Flow towards a Vertical Riga Plate in Hybrid Cu–Al<sub>2</sub>O<sub>3</sub>/Water Nanofluid. *Mathematics* **2020**, *8*, 912. [[CrossRef](#)]
22. Khashi'ie, N.S.; Arifin, N.M.; Pop, I.; Nazar, R.; Hafidzuddin, E.H.; Wahi, N. Flow and heat transfer past a permeable power-law deformable plate with orthogonal shear in a hybrid nanofluid. *Alex. Eng. J.* **2020**, *59*, 1869–1879. [[CrossRef](#)]
23. Khashi'ie, N.S.; Arifin, N.M.; Pop, I.; Nazar, R.; Hafidzuddin, E.H.; Wahi, N. Three-Dimensional Hybrid Nanofluid Flow and Heat Transfer past a Permeable Stretching/Shrinking Sheet with Velocity Slip and Convective Condition. *Chin. J. Phys.* **2020**, *66*, 157–171. [[CrossRef](#)]
24. Ali, I.; Alsabery, A.I.; Bakar, N.; Roslan, R. Mixed Convection in a Double Lid-Driven Cavity Filled with Hybrid Nanofluid by Using Finite Volume Method. *Symmetry* **2020**, *12*, 1977. [[CrossRef](#)]
25. Khan, M.R.; Pan, K.; Khan, A.U.; Nadeem, S. Dual solutions for mixed convection flow of SiO<sub>2</sub>–Al<sub>2</sub>O<sub>3</sub>/water hybrid nanofluid near the stagnation point over a curved surface. *Phys. A Stat. Mech. Appl.* **2020**, *547*, 123959. [[CrossRef](#)]
26. Liu, W.; Al-Rashed, A.A.; Alsagri, A.S.; Mahmoudi, B.; Shahsavari, A.; Afrand, M. Laminar forced convection performance of non-Newtonian water-CNT/Fe<sub>3</sub>O<sub>4</sub> nano-fluid inside a minichannel hairpin heat exchanger: Effect of inlet temperature. *Powder Technol.* **2019**, *354*, 247–258. [[CrossRef](#)]
27. Devi, S.U.; Devi, S.A. Heat transfer enhancement of Cu–Al<sub>2</sub>O<sub>3</sub>/water hybrid nanofluid flow over a stretching sheet. *J. Niger. Math. Soc.* **2017**, *36*, 419–433.
28. Takabi, B.; Salehi, S. Augmentation of the heat transfer performance of a sinusoidal corrugated enclosure by employing hybrid nanofluid. *Adv. Mech. Eng.* **2014**, *6*, 147059. [[CrossRef](#)]
29. Sheremet, M.A.; Cimpean, D.S.; Pop, I. Thermogravitational convection of hybrid nanofluid in a porous chamber with a central heat-conducting body. *Symmetry* **2020**, *12*, 593. [[CrossRef](#)]
30. Chamkha, A.J.; Mansour, M.A.; Rashad, A.M.; Kargarsharifabad, H.; Armaghani, T. Magneto-hydrodynamic mixed convection and entropy analysis of nanofluid in gamma-shaped porous cavity. *J. Thermophys. Heat Transf.* **2020**, *34*, 836–847. [[CrossRef](#)]
31. Alsabery, A.I.; Tayebi, T.; Roslan, R.; Chamkha, A.J.; Hashim, I. Entropy Generation and Mixed Convection Flow Inside a Wavy-Walled Enclosure Containing a Rotating Solid Cylinder and a Heat Source. *Entropy* **2020**, *22*, 606. [[CrossRef](#)]
32. Costa, V. Bejan's heatlines and masslines for convection visualization and analysis. *Appl. Mech. Rev.* **2006**, *59*, 126–145. [[CrossRef](#)]
33. Reddy, J.N.; Gartling, D.K. *The Finite Element Method in Heat Transfer and Fluid Dynamics*; CRC Press: Boca Raton, FL, USA, 2010.

34. Zienkiewicz, O.; Taylor, R.; Nithiarasu, P. The Finite Element Method. In *Fluid Dynamics*; Butterworth-Heinemann: Oxford, UK, 2005; Volume 3.
35. Nithiarasu, P.; Sundararajan, T.; Seetharamu, K. Finite element analysis of transient natural convection in an odd-shaped enclosure. *Int. J. Numer. Methods Heat Fluid Flow* **1998**, *8*, 199–216. [[CrossRef](#)]
36. Kahveci, K. Buoyancy driven heat transfer of nanofluids in a tilted enclosure. *J. Heat Transf.* **2010**, *132*, 062501. [[CrossRef](#)]
37. Ilis, G.G.; Mobedi, M.; Sunden, B. Effect of aspect ratio on entropy generation in a rectangular cavity with differentially heated vertical walls. *Int. Commun. Heat Mass Transf.* **2008**, *35*, 696–703. [[CrossRef](#)]
38. Deng, Q.-H.; Tang, G.-F. Numerical visualization of mass and heat transport for conjugate natural convection/heat conduction by streamline and heatline. *Int. J. Heat Mass Transf.* **2002**, *45*, 2373–2385. [[CrossRef](#)]